Fluorescence imaging with tailored light

Jialei Tang[1,2], Jinhan Ren[1,2] and Kyu Young Han[1,*]

[1]CREOL, The College of Optics and Photonics, University of Central Florida, Orlando, Florida, USA

[2]These authors contributed equally to this work.

*Corresponding author: kyhan@creol.ucf.edu

Abstract

Fluorescence microscopy has long been a valuable tool for biological and medical imaging. Control of optical parameters such as the amplitude, phase, polarization and propagation angle of light gives fluorescence imaging great capabilities ranging from super-resolution imaging to long-term real-time observation of living organisms. In this review, we discuss current fluorescence imaging techniques in terms of the use of tailored or structured light for the sample illumination and fluorescence detection, providing a clear overview of their working principles and capabilities.

1 Introduction

Fluorescence microscopy has been widely used in numerous biological applications because it provides molecular specificity via the labeling of target molecules with fluorescent probes [1, 2]. This allows one to systematically study the dynamic behavior of living cells and tissues, and to reveal fine structures of interest and their interactions with other biomolecules. Over the last two decades numerous fluorescence imaging techniques have been invented, expanding the capabilities of conventional imaging methods. For instance, subdiffraction spatial resolution was achieved by several far-field approaches, which enabled subcellular structures to be clearly imaged at the nanoscale [3]. Suppression of out-of-focus background light made it possible to directly observe and track single-molecules with high signal-to-background ratio (SBR), improving our understanding of molecular mechanisms [4] and providing an analytical means for quantitative measurements of gene expression [5]. The ability to perform long-term imaging with a low-light dose facilitated the investigation of developmental processes and neuronal activities on a large scale with unprecedented spatiotemporal resolution [6, 7].

One of the main factors that led to these advances in modern fluorescence microscopy is great progress in tailoring the illumination beam and the light emitted from the samples. Manipulating the fundamental properties of light, i.e. amplitude, phase or polarization allows the generation of a user-defined spot, line or plane depending on the imaging technique. Powerful optical devices such as deformable mirrors and spatial light modulators (SLM) offer a large degree of freedom to control beams [8] and especially make it possible to minimize aberrations induced by specimens and optical components [9, 10]. Specific arrangements of tailored beams can further enable desirable features by coherent/incoherent superposition, parallelization and time-averaging.

In this review, we will describe how tailored light has been applied to advanced state-of-art fluorescence imaging techniques regarding three main aspects: super-resolution microscopy, high contrast imaging with epi-illumination and fast volumetric imaging. We will explain their underlying principles based on how the beams are prepared at the back focal plane (BFP) of the objective lens. This will guide more explicit understanding in applying them to specific applications.

2 Super-resolution

2.1 Stimulated emission depletion (STED) microscopy

STED microscopy was first proposed to break the diffraction-limited spatial resolution in far-field fluorescence imaging [11, 12]. In this method, a tightly focused excitation beam is overlaid with what is referred to as the STED beam, which is red-shifted in the wavelength. The two beams are scanned over the sample, and the emitted fluorescence signal is registered at each coordinate. The STED

beam has a spatial distribution featuring a zero at the center of the beam such that it brings the excited fluorophores located in the peripheral regions of the excitation beam back to the ground state through stimulated emission before the spontaneous emission occurs. High intensity STED light induces saturation of the depletion of the fluorescent state, and this effectively narrows the point spread function (PSF).

Advancement of STED microscopy has been closely related to the use of sophisticated PSF engineering techniques. In the early days, an offset beam with a Gaussian profile was used to demonstrate that the STED mechanism indeed improves the spatial resolution [13]. In this case, the STED beam was displaced laterally with respect to the excitation beam, which provided a resolution improvement in 1D (x) on the focal plane [13] and along the optical axis [14]. Before long, it was suggested to use focal intensity distributions with a dark spot at the center by modulating the phase of the wavefront. A semi-circular π-shifting phase plate was employed for transforming a Gaussian beam (Figure 1A) to produce a central minimum line (Figure 1B), yielding a robust 1D-STED where the polarization of the STED light was parallel to the dividing line [15]. This pattern has been used for maximizing STED resolution down to a few nanometers [16]. It was straightforward to attain a lateral (x, y) resolution enhancement by coherently or incoherently adding two orthogonal semi-circular π-shifting phase plates in a Mach-Zehnder interferometer [15].

Alternatively, a circularly polarized Laguerre-Gaussian beam called a doughnut pattern was suggested to be used in STED microscopy [17, 18]. A Gaussian beam with a planar wavefront was converted to the doughnut pattern by applying a phase vortex to a SLM and then imaged at the BFP of objective lens [19]. The SLM was either directly imprinted with a vortex phase distribution ranging from 0 to 2π [19] (Figure 1C) or configured with an off-axis hologram that minimized the contribution of the unmodulated 0^{th} order beam [20]. Interestingly, this approach was shown to be immune to spherical aberration caused by refractive index mismatch in the sample [17, 21] and has a high depletion efficiency [22]. The availability of a polymeric vortex phase plate made the doughnut pattern widely used in STED microscopy [23]. This compact and affordable device exhibited high transmission efficiency (>95%) and a strong resistance to a high power CW laser, making it a standard beam shaping module in 2D-STED microscopy. Additionally, a liquid crystal device [24] and an optical vortex fiber [25] can also generate a doughnut pattern, which may facilitate the implementation of STED microscopy if the intensity at the doughnut center decreases further.

In contrast, an axial (z) resolution enhancement in STED microscopy was realized quite early by using a phase plate that had been used in optical trapping [26]. The central region of the phase plate imparted a phase delay of π, which induced destructive interference along the optical axis leading to what is called z-STED [27] (Figure 1H). While the z-STED technique primarily improves on-axis resolution, it also slightly improves the resolution in the lateral direction. Two incoherent de-excitation patterns, i.e. 2D-STED and z-STED can be superimposed upon each other [28] to yield a significantly reduced focal spot in 3D [29, 30].

More effective STED beams have been considered to improve the performance of STED microscopy in both 2D and 3D. The resolution of STED microscopy is described by an inverse square-root law, i.e., $d \approx \lambda/2\mathrm{NA}(1+\beta(I_m/I_S))^{1/2}$, where λ is the wavelength of fluorescence emission, NA is a numerical aperture of objective, I_m is the maximum intensity of the switch-off beam, and I_S is a characteristic intensity that can deplete half the fluorescence of fluorophores. Here, β is a geometrical factor and it displays a higher value when the slope near the center of the STED beam is steeper, i.e. it can deplete the fluorescence efficiently with a lower illumination intensity. Generally, the slope shows a quadratic dependence on x, y and z [23, 31]. In particular, cylindrical vector beams [32, 33] have been extensively investigated. These beams have spatially varying polarizations, leading to polarization vortices in contrast to phase vortices. One suggested method to achieve a finer lateral resolution with less illumination intensity was by an azimuthally polarized beam (Figure 1D) [34], or by the superposition of two azimuthally polarized beams where a binary phase plate (Figure 1E) is applied to one beam and a quadrant $0/\pi$ phase plate (Figure 1F) is applied to the other [35]. However, the azimuthally polarized beam is undesirable to STED imaging because its depletion efficiency is strongly

affected by the orientation of molecules [36], although this effect is often suppressed when the rotation of fluorophores is fast and/or many fluorophores reside within the subdiffraction spot. To generate uniform 3D de-excitation patterns, one approach was proposed by incoherently superimposing a radially polarized beam that is split and modulated with a quadrant 0/π phase plate (Figure 1G) along one path and with a π-shifted phase plate (Figure 1I) along the other path [37], but its effective PSF on the focal plane was non-uniform. Another approach was to use a higher-order radially polarized transverse electromagnetic mode (Figure 1J) and its variant modulated with a vortex phase plate (Figure 1K). This technique can potentially generate optical bottles or cages [38, 39] with isotropic 3D resolution.

Two interesting methods hybridized previous techniques to provide new features and capabilities. The first is a coherent hybrid depletion pattern called CH-STED [40]. The phase pattern consisted of two vortices, a disc and a ring, which had a same helicity but were out of phase (Figure 1M). They were reminiscent of an enlarged 2D-STED [41] and an annular vortex [42], respectively. CH-STED enabled high contrast STED imaging even at low or intermediate STED power by suppression of incomplete depletion of the out-of-focus background [43]. The second method is called easySTED and uses a different approach to create a 2D doughnut beam by using a quarter wave plate and a segmented half wave plate (Figure 1L) to manipulate the polarization of the STED beam [36]. The beam then becomes radially polarized by a quadrant 0/π phase plate for $\phi = 0$ (Figure 1G) and azimuthally polarized for $\phi = \pi/2$ (Figure 1E), where ϕ is the phase of STED beam. The segmented half wave plate was designed to be chromatic so the excitation beam is unaffected. easySTED facilitated the use of pre-aligned excitation and STED beams emanating from a single fiber without a degradation of the imaging performance, which made it possible to have an alignment-free STED system. A similar approach was demonstrated for easy z-STED [44].

A sharper excitation beam can also enhance the performance of STED microscopy. A radially polarized annular beam [45] or a circularly polarized beam with a binary amplitude filter [46] was known to show a laterally or axially tighter focus, respectively (Figure 2A, B, C). A recent study applied the former to STED microscopy and demonstrated that less STED power was required than the conventional approach to attain a similar resolution [47]. However, as this beam shows a significantly elongated excitation profile along the optical axis, it may suffer from a poor contrast due to incomplete depletion for 3D samples. Similar problems are expected if a super-oscillation based excitation beam [48, 49] is used in STED microscopy.

For imaging thick biological samples, it is crucial to properly manage aberrations that can reduce the resolution and signal-to-noise ratio (SNR) of images. To attain high quality STED images, it is important to keep the intensity at the center of the STED pattern close to zero; otherwise, the residual STED light adversely depletes the fluorescence. Typically the center needs to be <0.3% of the peak intensity of STED beam [16, 23]. z-STED has been known to be susceptible to aberrations, as contrasted with 2D-STED [17, 21]. For example, aberrations induced by a refractive index mismatch in the sample yield a considerable amount of residual light at deeper imaging depths with z-STED (Figure 3). A simple remedy is to use glycerol [50], silicone or water immersion objectives [51] for tissues or aqueous samples to minimize the refractive index difference between the immersion fluid and the sample. Adaptive optics has been used to fully compensate for specimen induced aberrations. For example, two SLMs have been used to correct the excitation and z-STED beams [52], and fluorescence detection was improved by a SLM and a deformable mirror [53]. This enabled the use of STED microscopy for imaging thick, strongly aberrating samples [54]. Furthermore, a single SLM has provided a convenient way to realize 3D-STED [55] and correct both the excitation and STED beams [56].

2.2 Structured illumination microscopy (SIM) and parallelized reversible saturable optical fluorescence transitions (RESOLFT) microscopy

SIM can achieve two-fold enhancement of the spatial resolution in a wide-field fluorescence microscope and is compatible with most standard fluorophores [57, 58]. The sample is illuminated with a series of known excitation patterns, such as sinusoidal grids with a corresponding phase shift for

each different pattern orientation [59, 60]. The high spatial frequency information is encoded into the observed images and can be recovered in post-processing.

The sinusoidal pattern is typically generated by a transmissive phase grating with an order selection mask, and the ±1 diffraction orders are focused onto the BFP of the objective (Figure 4A) [59, 60]. The illumination pattern is projected on the sample as the grating is translated and rotated. For high contrast SIM images, it is crucial to have a full modulation depth of the pattern, which is ensured by a linearly polarized beam whose direction is parallel to the stripe (s-polarization) [61]. This minimizes the residual light at the trough and prevents unwanted background noise. When total internal reflection fluorescence (TIRF) illumination was used to image near the surface (Figure 4B), SIM readily demonstrated ~100 nm resolution [62-64] and even sub-100 nm resolution with a high NA objective [65]. The principle has been extended in 3D-SIM to double the axial resolution as well as the lateral resolution, where a 3D interference pattern was generated by the 0 and ±1 diffraction orders (Figure 4C) with different illumination intensities [66]. It is desirable to use a slightly (spatially) incoherent light source to help time-average the speckle pattern and to phase out the 3D SIM pattern along the z-axis. This was accomplished by coupling light sources to a multimode fiber with a phase scrambler. Whereas random speckle patterns showed several merits in SIM [67, 68], they demanded a substantially large number of raw images compared to the standard SIM pattern and were not suitable to 3D biological imaging.

The mechanical movement of the physical grating slows down the imaging speed of SIM. However, this problem was solved by employing a SLM [69]. This could rapidly generate, translate and rotate the pattern, and a liquid crystal device was used to change the polarization state of the output beam from the SLM [64]. This approach demonstrated video-rate 2D-SIM [64] and fast volumetric SIM [70] in living cells. Recently, a segmented azimuthal polarizer was proposed to replace the liquid crystal phase retarder to provide a more viable method of preparing the s-polarization for all illumination patterns [71].

When imaging a thick fluorescent sample, wide-field SIM illumination generates considerable out-of-focus light which highly increases the background noise. As a result, the reconstructed images suffer from strong noise artifacts. Recently, SIM with sparse illumination patterns has been proposed to reject out-of-focus fluorescence, including line-scanning [72] (Figure 4D) and multifocal illumination [73, 74] (Figure 4E) systems. The latter was conveniently generated by a digital micromirror device or a spinning disk system without considering polarization state, and moreover enabled video-rate imaging [75, 76]; however, its resolution was not as good as traditional SIM [58]. Adaptive optics has seen limited use in SIM [77], but will enhance the resolution and contrast of multifocal SIM, especially when combined with two-photon excitation [78].

Structured illumination patterns can be applied in parallelized RESOLFT microscopy. RESOLFT uses fluorescent probes exhibiting reversible photoswitching between a bright and a dark state, and STED is one of its mechanisms [79, 80]. Since RESOLFT requires much lower light intensities than STED, it is possible to adapt a parallelized scanning scheme that fully benefits from fast, large field-of-view (FOV) imaging. Initially an 1D sinusoidal pattern was generated by an interferometer for proof-of-principle experiments of RESOLFT [81]. Recently, parallelized RESOLFT with more than 100,000 donuts has been achieved [82]. To implement this scheme, two orthogonally structured illumination patterns were incoherently superimposed on the sample plane (Figure 4F), serving as a fluorescence depletion pattern. Similar to SIM, the pattern was generated by a diffraction grating and it was suitable for multi-color imaging due to the independence of the grid pattern from the illumination wavelengths [83]. Parallelized STED microscopy with a 2D grid pattern was also demonstrated [84, 85] and in this case each standing wave pattern was formed from the interference of two inclined plane waves which is more efficient than a diffraction grating. Selective photoactivation by TIRF [86] or multifocal illumination [87] (Figure 4E) can enhance the contrast of parallelized RESOLFT images. A donut array [88] and a 3D depletion pattern based on the interference of five coherent beams (Figure 4G) [89] are likely to extend applications of parallelized STED/RESOLFT to fast 3D nanoscopy.

2.3 Single-molecule localization microscopy (SMLM)

A single fluorophore can be localized with high precision proportional to the inverse of the square root of the collected photons from the isolated single emitter [90]. Several techniques are able to isolate individual single-molecules within biological samples that are densely labeled with many fluorescent probes so that localization is possible. For example, a sparse subset of fluorophores can be activated by light that switches fluorophores between a fluorescent state and a dark state [91-93], or a subset of molecules can be sparsely targeted via the binding and unbinding of fluorescently labeled molecules [94, 95]. The SMLM image is then reconstructed from numerous subset images with nanometer localization accuracy [96].

In SMLM, the sample is typically illuminated by a large area beam such as epi- or TIRF-illumination. Other excitation schemes to guarantee high SNR in 3D single-molecule samples will be discussed in detail in Section 3. A few SMLM studies have used adaptive optics in the detection path to correct sample-induced aberrations [97, 98] and recent studies reported a significant increase of the localization precision in thick brain samples [99, 100].

Numerous SMLM studies have focused on the detection path, aiming to improve the axial localization precision by encoding the fluorescent emitter's depth information into the shape of PSF using phase aberrations. This includes an astigmatic PSF [101], rotating double-helix PSF (DH-PSF) [102], tetrapod PSF [103] and self-bending PSF [104]. The features of these PSFs vary distinctly as a function of defocusing depth [105]. The lateral and axial position of emitters can be extracted and characterized based on parameters specific to the tailored PSFs. For example, the variation of PSF width along the x and y axes for the astigmatic PSF (Figure 5A), the angle of two main lobes of the DH-PSF (Figure 5B) or relative stretching of the two lobes along the lateral direction for the self-bending PSF. The axial position of the emitter is then determined by a calibration curve linked to these parameters, and the lateral position is calculated in the same manner as other localization methods. One should carefully select the proper PSF for their application according to the wide-ranging performance in terms of size and axial range. For instance, the astigmatic PSF has much smaller axial range than that of the DH-PSF (~2-3 μm), and the Tetrapod PSF has even larger range up to 6 μm at the expense of a larger footprint [105].

3 Background suppression for fast and high contrast imaging with epi-illumination

3.1 Widefield and total internal reflection fluorescence (TIRF) microscopy

Epi-illumination widefield fluorescence microscopy has been the most common imaging technique for biological and clinical applications. For example, many super-resolution imaging methods discussed in section 2 including SIM, parallelized RESOLFT and SMLM indeed use a widefield approach. While for confocal microscopy a collimated beam is tightly focused by an objective (Figure 6A), for widefield microscopy the whole volume of the sample is uniformly illuminated (Figure 6B) by focusing a beam to the center of objective's back focal plane (BFP) or pupil plane. This allows fast imaging with relatively gentle illumination. The main drawback of widefield microscopy is the lack of optical sectioning capability. Although its depth of field is <1 μm when a high NA objective is used, the out-of-focus background greatly degrades the SBR of targets of interest. Deconvolution [106] and incoherent structured illumination [107] are efficient means to achieve 3D imaging capability with widefield microscopy, but they are not suitable to study weakly fluorescent samples and thus limitedly used for thin and bright specimens.

A confined illumination near the sample surface can be provided by TIRF microscopy [108]. When the incidence beam reaches to a critical angle, total internal reflection (TIR) occurs at the glass/water interface which generates an evanescent wave that excites fluorophores within the penetration depth of ~100-200 nm. This feature makes TIRF illumination an ideal tool for monitoring cellular dynamics with high contrast at the cell surface [109] and performing single-molecule experiments [110]. For TIR generation, a beam is tightly focused close to the edge of the pupil of a high NA objective (Figure 6C). Since the available annulus width for TIR generation at the BFP is relatively small, a light source with

high spatial coherence is needed for objective type TIRF imaging. Note that there are other methods to generate TIRF, e.g. prisms [111] or waveguides [112, 113].

TIRF microscopy often suffers from inhomogeneous spatial illumination attributed to two main causes. The first is a speckle fringe produced by interference from the laser light that is scattered or reflected from the sample and optical components. This unevenness can be eliminated by rotating a focused beam along the annulus of the BFP (Figure 6D) [114-116]. In this way, the illumination is time-averaged. The second cause is a Gaussian-shaped beam. Many approaches that improved the illumination flatness in epi-illumination [117, 118] are inadequate to be used in TIRF microscopy because of their poor spatial coherence. This has recently been resolved by refractive optics-based beam shaping tools [119, 120]. This showed significant improvements in quantitative single-molecule analysis [119] and uniform resolution in SMLM with large imaging areas [121].

Another challenge of TIRF is a nonevanescent excitation that comes from scattering of the evanescent wave due to the nonuniform refractive index in cellular environments [122]. To suppress background fluorescence by far-field excitation, it was suggested to monitor supercritical angle fluorescence (SAF) [123] which used the fact that the fluorescence emission near the sample interface preferentially orients to high angles on the BFP [124]. SAF is regarded as a counterpart of TIRF illumination [108]. Since the PSF of the SAF is broader laterally, it is undesirable to use it directly. Instead, image subtraction of undercritical light from all the emission components provides high resolution TIRF, so-called virtual SAF microscopy (Figure 6E) [125]. Another approach to obtain clear TIRF images is to apply incoherent structured illumination patterns, yielding widefield microscopy with improved optical sectioning [126].

3.2 Highly inclined illumination

Since TIRF microscopy has a limited excitation depth, it is highly desirable to seek alternatives that enable imaging inside cells and tissues with single-molecule sensitivity. When the focused spot under a TIRF condition is slightly shifted at the BFP such that the illumination gets very close to the critical angle, a pseudo TIRF or grazing incidence illumination is generated (Figure 6F) [127, 128]. Its illumination depth (~1 μm) is particularly useful to study structures and dynamics of subcellular organelles that are positioned near the surface. Basically, this approach utilizes a leaky far-field evanescent wave for excitation. To obtain a deeper imaging depth, for example, to visualize the entire nucleus of mammalian cells, the focused spot is further shifted toward the center of the BFP. In this case, a collimated beam refracted at the glass/water interface is propagated with an inclined angle (θ) with respect to the z axis (Figure 6G). Specially, if the inclined angle is high, e.g. $\theta > 75°$, a thin off-axis light sheet is generated, which significantly reduces out-of-focus background. This technique, called highly inclined and laminated optical sheet (HILO) microscopy [129, 130], has been widely used for 3D super-resolution imaging [131] and single-molecule analysis [132]. It is also possible to switch between TIRF and HILO illuminations by rapidly changing the beam position at the BFP [133]. Interestingly, despite its simple working principle, HILO imaging was reported more than two decades after TIRF microscopy was first demonstrated.

One drawback of HILO is that its beam thickness (Δz) is closely related to the imaging FOV. If aberrations are neglected, the beam thickness is roughly calculated as $\Delta z = D/\tan(\theta)$, where D is the beam diameter. It means that a thinner illumination unavoidably results in a smaller illumination area, which greatly limits its applications. Therefore the commonly used HILO beam is relatively thick, about 5-7 μm. This problem has been recently resolved by highly inclined swept tile (HIST) microscopy [134]. An elongated beam prepared by a pair of cylindrical lenses is focused on the BFP of the objective similar to HILO. Then a virtual light sheet is generated by laterally sweeping the tile beam and a confocal slit removes out-of-focus fluorescence (Figure 6H). In this way, HIST decoupled the beam thickness from the FOV and successfully demonstrated large area 3D single-molecule imaging in the presence of high background [134]. Note that an instantaneous illumination intensity of HIST is just 5-10 times higher than TIRF so it can be considered as gentle illumination. It is feasible to further decrease the beam thickness and extend the imaging depth by utilizing adaptive optics [9] and PSF engineering [105], which will enhance contrast and minimize unwanted excitation.

3.3 Parallelized illumination and line-scanning confocal microscopy

Confocal microscopy provides tightly focused illumination and its pinhole effectively removes out-of-focus background [135]. Nevertheless, due to its high illumination intensity, confocal microscopy has been used mostly when the sample is strongly fluorescent and relatively insensitive to photobleaching and photodamage, which depend on the peak excitation intensity given the same light dose [136]. To lower the excitation intensity and speed up the imaging acquisition time, it was proposed to use parallelized illumination instead of single-spot scanning. One approach called spinning disk confocal microscopy generates multifocal spots [137, 138] by a Nipkow-type pinhole array disk and a microlens array [139], and the generated signal is projected onto a camera. Its pattern is similar to multifocal SIM shown in Figure 4E, but has an equal-pitch spiral shape to ensure the beam uniformity. Video-rate imaging is accomplished by illuminating the sample with more than a few hundred foci [140]. Contrary to expectations, the optical sectioning of spinning disk system is substantially degraded by inevitable crosstalk between adjacent pinholes [141] unless multiphoton excitation is applied [142]. This drawback was mitigated by increasing the pitch between foci and decreasing the pinhole size, but this worsened the degree of parallelization [143].

Line illumination is another way to parallelize the excitation beam [144, 145]. A beam focused in one direction is scanned over the sample (Figure 6I), and a slit instead of a pinhole renders moderate optical sectioning, i.e. its out-of-focus background scales with ~$1/z$ as contrasted with ~$1/z^2$ for the single spot scanning confocal microscopy. Because of this, line-scanning confocal microscopy (LS) has not been popularly used in fluorescence imaging. However, a systematic comparison between spinning disk and LS revealed that LS indeed showed higher sensitivity and better depth discrimination (Figure 7) [146, 147]. Since then many applications have been demonstrated, including SMLM in cells and thick tissues [148, 149] and fast imaging of large specimens for histopathology [150, 151]. The biggest advantage of LS is its simplicity [152]. Line illumination was also used in real-time two-photon imaging [153].

When the line illumination is titled with respect to the z-axis (Figure 6J) the excitation area gets wider, which slightly degrades spatial resolution but results in similar effects as parallelization. This technique showed reduced photobleaching while maintaining a similar optical sectioning to conventional LS [154]. The instantaneous intensity required to maintain the same SBR can be lowered by using multiple inclined beams distantly spaced from each other. This inclined line-scanning confocal microscopy can be regarded as a special case of HIST microscopy with a very thin illumination beam.

4 Fast volumetric imaging

4.1 Extended FOV and high resolution in light-sheet fluorescence microscopy (LSFM)

Confocal microscopy and other epi-illumination approaches provide good sectioning capability; however, they excite fluorophores in unwanted volumes, which leads to unavoidable photobleaching and phototoxicity in living biological samples. LSFM selectively excites the target of interest in the vicinity of imaging plane with an additional orthogonally placed objective lens [155-157], which maximizes the usable excitation photons for 3D time-lapse imaging [158]. Due to its capability of fast, gentle and long-term imaging [157], LSFM has shown remarkable success in diverse areas.

Typically a cylindrical lens was used to shape the Gaussian beam into a light-sheet for the sample excitation (Figure 8A), and the emitted fluorescence was detected by a large FOV camera [157]. To get a more uniform illumination a focused laser beam was digitally scanned to form a time-averaged virtual light-sheet (Figure 8B) [159], but this approach required at least two orders of magnitude higher instantaneous illumination intensity than the former. In LSFM, non-uniformity due to strong absorption and scattering often occurs in the illumination, resulting in image artifacts such as stripes and shadows. This problem was alleviated by multidirectional illumination and reconstruction of these images [160, 161]. Another shortcoming of LSFM is that the available FOV, governed by the Rayleigh length of a propagating Gaussian beam, is coupled with the thickness of the illumination beam, i.e. $y_R = \pi \cdot \omega_0^2/\lambda$, where y_R denotes the Rayleigh length, ω_0 the beam waist and λ the excitation wavelength. Therefore,

it is not feasible to conduct high-resolution subcellular imaging across a large FOV with a tightly confined Gaussian beam (Figure 8A).

To overcome this problem an extended and uniform light-sheet was generated by scanning a Bessel beam [162], projected by an annular illumination at objective's BFP [163, 164] using a SLM or an axicon [165, 166] (Figure 8C). The Bessel beam features an invariant transverse profile as well as self-reconstruction that suppresses artifacts from scattering. Nevertheless, its narrow center peak is accompanied by strong side lobes, which generates substantial out-of-focus background [164]. This was reduced by structured illumination, two-photon excitation or a confocal slit [164, 167, 168]. Later, a lattice light-sheet was introduced by dithering a Bessel beam array that was carefully designed to be destructively interfered [169] to effectively suppress the side lobes (Figure 8D) [170]. Due to its thin illumination across large FOV, lattice light-sheet microscopy enables high-resolution long-term live-cell imaging with an extremely low light dose and is regarded as an ideal fluorescence imaging system for many biological studies. Alternatively, it was proposed to use pseudo-nondiffracting beams featuring attenuated side lobes by superimposing two coaxial Bessel beams [171, 172] (Figure 8E) or two cosine-Gauss beams [173, 174] (Figure 8F). However, they showed either a rather limited FOV or a relatively thicker beam as contrasted with the lattice light-sheet. Similarly, an Airy beam [175] was also used for LSFM with a cubic phase mask [176] but it is unlikely to be suitable to high-resolution imaging [158]. The second strategy to attain high contrast LSFM imaging with a large FOV is to sweep or tile Gaussian beams. For example, in axially swept light-sheet microscopy, a light-sheet with a small Rayleigh length was rapidly scanned over large specimens by defocusing the beam in conjunction with a confocal slit for background rejection, resulting in a thin virtual light-sheet [177]. Another approach is to stitch multiple images generated by light-sheets via the Gaussian beam [178].

Many LSFM techniques use virtually generated light-sheets. As discussed earlier, they require much higher peak excitation power. Similar to epi-illumination, parallelization of the beam can lower the peak power without sacrificing imaging speed [179]. Recently, a new approach called field synthesis was demonstrated which can generate any scanned or dithered light sheet [180]. Whereas conventional methods scanned the beam laterally on the sample plane, for field synthesis a focused line was scanned over the objective BFP which generated instantaneous light-sheet patterns accordingly (Figure 8G). As the illumination profile at any moment covers almost the same excitation area, field synthesis ensured a much lower peak illumination intensity, or in other words, less photobleaching and photodamage to samples [180]. Similarly, it was also reported to use a line Bessel sheet using a slit and annular ring mask [181].

Other illumination schemes can be combined with LSFM to increase spatial resolution, such as SIM [65, 170, 182] and STED/RESOLFT [183, 184]. Adaptive optics has also shown to be useful for correcting illumination and/or detection to clearly visualize thick specimens [185-187]. On the other hand, the requirement of two closely placed objectives has greatly limited the available NA for both the excitation and fluorescence detection, especially preventing the observation of single-molecules with high SNR [188, 189]. Many approaches have solved this problem by introducing new excitation arrangements [190], for example, the addition of a small reflective device in the sample chamber [191], the design of special sample holders [192-195], or the usage of auxiliary optics [174, 196] for delivering a thin light-sheet into the sample. Alternatively, single objective-based LSFM has emerged to circumvent this issue. This approach used inclined illumination in a standard microscope, but an additional two objectives were used to relay an intermediate image with minimal spherical aberration and to set the image on the focal plane by tilting the last objective [197, 198]. Recently, the low detection efficiency of single objective LSFM has been significantly improved by extending the collection angle [199, 200].

4.2 Extended imaging depth for *in vivo* imaging

Although LSFM enables fast volumetric imaging with a minimal light dose, it has limitations when studying opaque samples, such as mammalian brains and when interrogating awake mice [201]. In this case, two-photon excitation laser scanning microscopy has provided a solution to suppress the strong scattering and facilitate its implementation to study freely behaving animals [202, 203]. However,

since this is still a point scanning technique, various beam shaping approaches have been developed to achieve fast volumetric imaging, particularly toward less or no serial z-scanning.

One approach is to use an elongated excitation by generating a Bessel beam and collecting the fluorescence signal from the illuminated volume [204, 205]. Since targets of interest in neuroscience are usually sparsely distributed, it is unlikely that each feature is excited by the elongated beam at the same time. Scanning the Bessel beam on the x-y plane gives a 2D projected image of the 3D sample at a video rate, which makes it unnecessary to obtain multiple z-stacks. Instead of the axially extended beam, it is possible to acquire several 2D images simultaneously at different focal planes by generating multiple beamlets at different depths [206]. In this case, slightly different temporal profiles of each beamlet made them distinguishable.

Other approach is to use temporal focusing [207, 208]. When ultrafast pulses broadened by a diffraction grating are imaged on the sample through a lens and objective, two-photon excitation occurs dominantly on the focal plane. This effectively sharpens the excitation beam along the z-axis and the depth of field can be tuned irrespective of the lateral PSF by changing the temporal profile of the pulses [207]. In addition, the temporal focusing has shown resistance to scattering in tissues [209, 210]. These great features have been combined with line-illumination [211-213] and wide-field illumination [207, 214] for fast volumetric two-photon imaging. If high spatial resolution is not required, for example, when observing mouse brains with a single neuron resolution, the excitation beam can be shaped to an isotropic PSF with a few microns in size, which was not attainable by a Gaussian beam [215]. This illumination extends the imaging depth and achieves considerable lateral parallelization.

An extended imaging depth can also be achieved by engineering the detection PSF. One simple implementation is to encode the wavefront in the back focal plane using a cubic phase mask which shows a defocus invariance [216]. The whole volume excited by epi-illumination [217] or light-sheet illumination [218] was projected to a single 2D image by this phase mask. However, the resulting images contained a substantial amount of side lobes, necessitating careful deconvolution and making the images immensely dim. Alternatively, it was proposed to image multiple focal planes in a single exposure of the camera [219]. A distorted diffraction grating [220] was designed to split fluorescence light depending on the degree of defocus. Whereas it enabled one to monitor nine focal planes simultaneously, the divided fluorescence signal lowered the SNR [221].

5 Conclusions

Myriads of new fluorescence imaging techniques have advanced imaging performance in terms of spatial resolution, SNR, 3D contrast, imaging speed and photodamage. Unfortunately, there are no magic bullets in fluorescence microscopy. Each method has its own pros and cons, and thus one needs to choose the proper imaging tool depending on their specific application. Notably, tailored beams have been critical drivers to success and often provided a breakthrough. Tailored beams have gained notable attention and have played important roles in other research areas [222], including material fabrication [223, 224], optical manipulations [225], microfluidics [226], optogenetics [227], etc. We envision that novel structured beams will provide fluorescence imaging with new functions and extend its applications to new research areas.

Funding

This work was supported by the National Science Foundation (1805200) and the National Institutes of Health (R21GM131163).

Acknowledgement

We thank Benjamin Croop for critically reading our manuscript.

References

[1] Lichtman JW, Conchello JA, Fluorescence microscopy, Nat. Methods **2**, 910-919 (2005).
[2] Pawley JB, Handbook of biological confocal microscopy, 3rd ed. Plenum Press, New York, USA, 2006.
[3] Schermelleh L, Ferrand A, Huser T, et al., Super-resolution microscopy demystified, Nat. Cell Biol. **21**, 72-84 (2019).
[4] Liu Z, Lavis LD, Betzig E, Imaging live-cell dynamics and structure at the single-molecule level, Mol. Cell **58**, 644-659 (2015).
[5] Crosetto N, Bienko M, van Oudenaarden A, Spatially resolved transcriptomics and beyond, Nat. Rev. Genet. **16**, 57-66 (2015).
[6] Huisken J, Stainier DYR, Selective plane illumination microscopy techniques in developmental biology, Development **136**, 1963-1975 (2009).
[7] Keller PJ, Ahrens MB, Visualizing whole-brain activity and development at the single-cell level using light-sheet microscopy, Neuron **85**, 462-483 (2015).
[8] Kubby JA, Adaptive optics for biological imaging CRC Press, Boca Raton, 2013.
[9] Booth MJ, Adaptive optical microscopy: the ongoing quest for a perfect image, Light Sci. Appl. **3**, e165 (2014).
[10] Ji N, Adaptive optical fluorescence microscopy, Nat. Methods **14**, 374-380 (2017).
[11] Hell SW, Wichmann J, Breaking the diffraction resolution limit by stimulated-emission - Stimulated-emission-depletion fluorescence microscopy, Opt. Lett. **19**, 780-782 (1994).
[12] Vicidomini G, Bianchini P, Diaspro A, STED super-resolved microscopy, Nat. Methods **15**, 173-182 (2018).
[13] Klar TA, Hell SW, Subdiffraction resolution in far-field fluorescence microscopy, Opt. Lett. **24**, 954-956 (1999).
[14] Klar TA, Dyba M, Hell SW, Stimulated emission depletion microscopy with an offset depleting beam, Appl. Phys. Lett. **78**, 393-395 (2001).
[15] Klar TA, Engel E, Hell SW, Breaking Abbe's diffraction resolution limit in fluorescence microscopy with stimulated emission depletion beams of various shapes, Phys. Rev. E **64**, 066613 (2001).
[16] Rittweger E, Han KY, Irvine SE, Eggeling C, Hell SW, STED microscopy reveals crystal colour centres with nanometric resolution, Nat. Photon. **3**, 144-147 (2009).
[17] Torok P, Munro PRT, The use of Gauss-Laguerre vector beams in STED microscopy, Opt. Express **12**, 3605-3617 (2004).
[18] Bokor N, Iketaki Y, Watanabe T, Fujii M, Investigation of polarization effects for high-numerical-aperture first-order Laguerre-Gaussian beams by 2D scanning with a single fluorescent microbead, Opt. Express **13**, 10440-10447 (2005).
[19] Willig KI, Rizzoli SO, Westphal V, Jahn R, Hell SW, STED microscopy reveals that synaptotagmin remains clustered after synaptic vesicle exocytosis, Nature **440**, 935-939 (2006).
[20] Auksorius E, Boruah BR, Dunsby C, et al., Stimulated emission depletion microscopy with a supercontinuum source and fluorescence lifetime imaging, Opt. Lett. **33**, 113-115 (2008).
[21] Deng SH, Liu L, Cheng Y, Li RX, Xu ZZ, Investigation of the influence of the aberration induced by a plane interface on STED microscopy, Opt. Express **17**, 1714-1725 (2009).
[22] Keller J, Schonle A, Hell SW, Efficient fluorescence inhibition patterns for RESOLFT microscopy, Opt. Express **15**, 3361-3371 (2007).
[23] Harke B, Keller J, Ullal CK, et al., Resolution scaling in STED microscopy, Opt. Express **16**, 4154-4162 (2008).
[24] Otomo K, Hibi T, Kozawa Y, et al., Two-photon excitation STED microscopy by utilizing transmissive liquid crystal devices, Opt. Express **22**, 28215-28221 (2014).
[25] Yan L, Kristensen P, Ramachandran S, Vortex fibers for STED microscopy, APL Photonics **4**, 022903 (2019).
[26] Ozeri R, Khaykovich L, Davidson N, Long spin relaxation times in a single-beam blue-detuned optical trap, Phys. Rev. A **59**, R1750-R1753 (1999).
[27] Klar TA, Jakobs S, Dyba M, Egner A, Hell SW, Fluorescence microscopy with diffraction resolution barrier broken by stimulated emission, Proc. Natl. Acad. Sci. U.S.A. **97**, 8206-8210 (2000).
[28] Bokor N, Davidson N, A three dimensional dark focal spot uniformly surrounded by light, Opt. Comm. **279**, 229-234 (2007).
[29] Harke B, Ullal CK, Keller J, Hell SW, Three-dimensional nanoscopy of colloidal crystals, Nano Lett. **8**, 1309-1313 (2008).
[30] Han KY, Ha T, Dual-color three-dimensional STED microscopy with a single high-repetition-rate laser, Opt. Lett. **40**, 2653-2656 (2015).
[31] Bokor N, Davidson N, Tight parabolic dark spot with high numerical aperture focusing with a circular pi phase plate, Opt. Comm. **270**, 145-150 (2007).
[32] Youngworth KS, Brown TG, Focusing of high numerical aperture cylindrical-vector beams, Opt. Express **7**, 77-87 (2000).
[33] Zhan QW, Cylindrical vector beams: from mathematical concepts to applications, Adv. Opt. Photonics **1**, 1-57 (2009).
[34] Hao XA, Kuang CF, Wang TT, Liu X, Effects of polarization on the de-excitation dark focal spot in STED microscopy, J. Opt. **12**, 115707 (2010).
[35] Xue Y, Kuang CF, Li S, Gu ZT, Liu X, Sharper fluorescent super-resolution spot generated by azimuthally polarized beam in STED microscopy, Opt. Express **20**, 17653-17666 (2012).

[36] Reuss M, Engelhardt J, Hell SW, Birefringent device converts a standard scanning microscope into a STED microscope that also maps molecular orientation, Opt. Express **18**, 1049-1058 (2010).
[37] Xue Y, Kuang CF, Hao X, Gu ZT, Liu X, A method for generating a three-dimensional dark spot using a radially polarized beam, J. Opt. **13**, 125704 (2011).
[38] Kozawa Y, Sato S, Focusing property of a double-ring-shaped radially polarized beam, Opt. Lett. **31**, 820-822 (2006).
[39] Man ZS, Bai ZD, Li JJ, et al., Optical cage generated by azimuthal- and radial-variant vector beams, Appl. Opt. **57**, 3592-3597 (2018).
[40] Pereira A, Sousa M, Almeida AC, et al., Coherent-hybrid STED: high contrast sub diffraction imaging using a bi-vortex depletion beam, Opt. Express **27**, 8092-8111 (2019).
[41] Hein B, Willig KI, Hell SW, Stimulated emission depletion (STED) nanoscopy of a fluorescent protein-labeled organelle inside a living cell, Proc. Natl. Acad. Sci. U.S.A. **105**, 14271-14276 (2008).
[42] Wang B, Shi JM, Zhang TY, et al., Improved lateral resolution with an annular vortex depletion beam in STED microscopy, Opt. Lett. **42**, 4885-4888 (2017).
[43] Ma Y, Ha T, Fight against background noise in stimulated emission depletion nanoscopy, Phys. Biol. **16**, 051002 (2019).
[44] Iketaki Y, Kumagai H, Jahn K, Bokor N, Creation of a three-dimensional spherical fluorescence spot for super-resolution microscopy using a two-color annular hybrid wave plate, Opt. Lett. **40**, 1057-1060 (2015).
[45] Dorn R, Quabis S, Leuchs G, Sharper focus for a radially polarized light beam, Phys. Rev. Lett. **91**, 233901 (2003).
[46] Neil MAA, Juskaitis R, Wilson T, Laczik ZJ, Sarafis V, Optimized pupil-plane filters for confocal microscope point-spread function engineering, Opt. Lett. **25**, 245-247 (2000).
[47] Lim G, Kim W, Oh S, Lee H, Park N, Enhanced lateral resolution in CW STED microscopy using tightly focused annular radially polarized excitation beam, J. Biophotonics **12**, e201900060 (2019).
[48] Kozawa Y, Matsunaga D, Sato S, Superresolution imaging via superoscillation focusing of a radially polarized beam, Optica **5**, 86-92 (2018).
[49] Gbur G, Using superoscillations for superresolved imaging and subwavelength focusing, Nanophotonics **8**, 205-225 (2019).
[50] Urban NT, Willig KI, Hell SW, Nagerl UV, STED nanoscopy of actin dynamics in synapses deep inside living brain slices, Biophys. J. **101**, 1277-1284 (2011).
[51] Heine J, Wurm CA, Keller-Findeisen J, et al., Three dimensional live-cell STED microscopy at increased depth using a water immersion objective, Rev. Sci. Instrum. **89**, 053701 (2018).
[52] Gould TJ, Burke D, Bewersdorf J, Booth MJ, Adaptive optics enables 3D STED microscopy in aberrating specimens, Opt. Express **20**, 20998-21009 (2012).
[53] Patton BR, Burke D, Owald D, et al., Three-dimensional STED microscopy of aberrating tissue using dual adaptive optics, Opt. Express **24**, 8862-8876 (2016).
[54] Zdankowski P, McGloin D, Swedlow JR, Full volume super-resolution imaging of thick mitotic spindle using 3D AO STED microscope, Biomed. Opt. Express **10**, 1999-2009 (2019).
[55] Lenz MO, Sinclair HG, Savell A, et al., 3-D stimulated emission depletion microscopy with programmable aberration correction, J. Biophotonics **7**, 29-36 (2014).
[56] Gorlitz F, Guldbrand S, Runcorn TH, et al., easySLM-STED: Stimulated emission depletion microscopy with aberration correction, extended field of view and multiple beam scanning, J. Biophotonics **11**, e201800087 (2018).
[57] Heintzmann R, Huser T, Super-Resolution Structured Illumination Microscopy, Chem. Rev. **117**, 13890-13908 (2017).
[58] Wu YC, Shroff H, Faster, sharper, and deeper: structured illumination microscopy for biological imaging, Nat. Methods **15**, 1011-1019 (2018).
[59] Heintzmann R, Cremer C, Laterally modulated excitation microscopy: improvement of resolution by using a diffraction grating, Proc. SPIE **3568**, 185-195 (1999).
[60] Gustafsson MGL, Surpassing the lateral resolution limit by a factor of two using structured illumination microscopy, J. Microscopy **198**, 82-87 (2000).
[61] Best G, Amberger R, Cremer C, "Super-Resolution Microscopy: Interference and Pattern Techniques," in *Fluorescence Microscopy: From Principles to Biological Applications*, U. Kubitscheck, ed. (2013), pp. 345-374.
[62] Frohn JT, Knapp HF, Stemmer A, True optical resolution beyond the Rayleigh limit achieved by standing wave illumination, Proc. Natl. Acad. Sci. U.S.A. **97**, 7232-7236 (2000).
[63] Fiolka R, Beck M, Stemmer A, Structured illumination in total internal reflection fluorescence microscopy using a spatial light modulator, Opt. Lett. **33**, 1629-1631 (2008).
[64] Kner P, Chhun BB, Griffis ER, Winoto L, Gustafsson MGL, Super-resolution video microscopy of live cells by structured illumination, Nat. Methods **6**, 339-342 (2009).
[65] Li D, Shao L, Chen BC, et al., Extended-resolution structured illumination imaging of endocytic and cytoskeletal dynamics, Science **349**, aab3500 (2015).
[66] Gustafsson MGL, Shao L, Carlton PM, et al., Three-dimensional resolution doubling in wide-field fluorescence microscopy by structured illumination, Biophys. J. **94**, 4957-4970 (2008).

[67] Mudry E, Belkebir K, Girard J, et al., Structured illumination microscopy using unknown speckle patterns, Nat. Photon. **6**, 312-315 (2012).
[68] Min J, Jang J, Keum D, et al., Fluorescent microscopy beyond diffraction limits using speckle illumination and joint support recovery, Sci. Rep. **3**(2013).
[69] Hirvonen LM, Wicker K, Mandula O, Heintzmann R, Structured illumination microscopy of a living cell, Eur. Biophys. J. **38**, 807-812 (2009).
[70] Shao L, Kner P, Rego EH, Gustafsson MGL, Super-resolution 3D microscopy of live whole cells using structured illumination, Nat. Methods **8**, 1044-1046 (2011).
[71] Foerster R, Lu-Walther HW, Jost A, et al., Simple structured illumination microscope setup with high acquisition speed by using a spatial light modulator, Opt. Express **22**, 20663-20677 (2014).
[72] Mandula O, Kielhorn M, Wicker K, et al., Line scan - structured illumination microscopy super-resolution imaging in thick fluorescent samples, Opt. Express **20**, 24167-24174 (2012).
[73] York AG, Parekh SH, Nogare DD, et al., Resolution doubling in live, multicellular organisms via multifocal structured illumination microscopy, Nat. Methods **9**, 749-754 (2012).
[74] Schulz O, Pieper C, Clever M, et al., Resolution doubling in fluorescence microscopy with confocal spinning-disk image scanning microscopy, Proc. Natl. Acad. Sci. U.S.A. **110**, 21000-21005 (2013).
[75] York AG, Chandris P, Nogare DD, et al., Instant super-resolution imaging in live cells and embryos via analog image processing, Nat. Methods **10**, 1122-1126 (2013).
[76] Azuma T, Kei T, Super-resolution spinning-disk confocal microscopy using optical photon reassignment, Opt. Express **23**, 15003-15011 (2015).
[77] Thomas B, Wolstenholme A, Chaudhari SN, Kipreos ET, Kner P, Enhanced resolution through thick tissue with structured illumination and adaptive optics, J. Biomed. Opt. **20**, 026006 (2015).
[78] Ingaramo M, York AG, Wawrzusin P, et al., Two-photon excitation improves multifocal structured illumination microscopy in thick scattering tissue, Proc. Natl. Acad. Sci. U.S.A. **111**, 5254-5259 (2014).
[79] Hell SW, Jakobs S, Kastrup L, Imaging and writing at the nanoscale with focused visible light through saturable optical transitions, Appl. Phys. A **77**, 859-860 (2003).
[80] Hofmann M, Eggeling C, Jakobs S, Hell SW, Breaking the diffraction barrier in fluorescence microscopy at low light intensities by using reversibly photoswitchable proteins, Proc. Natl. Acad. Sci. U.S.A. **102**, 17565-17569 (2005).
[81] Schwentker MA, Bock H, Hofmann M, et al., Wide-field subdiffraction RESOLFT microscopy using fluorescent protein photoswitching, Micr. Res. Tech. **70**, 269-280 (2007).
[82] Chmyrov A, Keller J, Grotjohann T, et al., Nanoscopy with more than 100,000 'doughnuts', Nat. Methods **10**, 737-740 (2013).
[83] Chmyrov A, Leutenegger M, Grotjohann T, et al., Achromatic light patterning and improved image reconstruction for parallelized RESOLFT nanoscopy, Sci. Rep. **7**, 44619 (2017).
[84] Yang B, Przybilla F, Mestre M, Trebbia JB, Lounis B, Large parallelization of STED nanoscopy using optical lattices, Opt. Express **22**, 5581-5589 (2014).
[85] Bergermann F, Alber L, Sahl SJ, Engelhardt J, Hell SW, 2000-fold parallelized dual-color STED fluorescence nanoscopy, Opt. Express **23**, 211-223 (2015).
[86] Chung E, Kim D, Cui Y, Kim YH, So PTC, Two-dimensional standing wave total internal reflection fluorescence microscopy: Superresolution imaging of single molecular and biological specimens, Biophys. J. **93**, 1747-1757 (2007).
[87] Masullo LA, Boden A, Pennacchietti F, et al., Enhanced photon collection enables four dimensional fluorescence nanoscopy of living systems, Nat. Comm. **9**, 3281 (2018).
[88] Zhekova M, Maleshkov G, Stoyanov L, et al., Formation of multi-spot focal arrays by square-shaped optical vortex lattices, Opt. Comm. **449**, 110-116 (2019).
[89] Xue Y, So PTC, Three-dimensional super-resolution high-throughput imaging by structured illumination STED microscopy, Opt. Express **26**, 20920-20928 (2018).
[90] Thompson RE, Larson DR, Webb WW, Precise nanometer localization analysis for individual fluorescent probes, Biophys. J. **82**, 2775-2783 (2002).
[91] Betzig E, Patterson GH, Sougrat R, et al., Imaging intracellular fluorescent proteins at nanometer resolution, Science **313**, 1642-1645 (2006).
[92] Rust MJ, Bates M, Zhuang XW, Sub-diffraction-limit imaging by stochastic optical reconstruction microscopy (STORM), Nat. Methods **3**, 793-795 (2006).
[93] Hess ST, Girirajan TPK, Mason MD, Ultra-high resolution imaging by fluorescence photoactivation localization microscopy, Biophys. J. **91**, 4258-4272 (2006).
[94] Sharonov A, Hochstrasser RM, Wide-field subdiffraction imaging by accumulated binding of diffusing probes, Proc. Natl. Acad. Sci. U.S.A. **103**, 18911-18916 (2006).
[95] Jungmann R, Steinhauer C, Scheible M, et al., Single-molecule kinetics and super-resolution microscopy by fluorescence imaging of transient binding on DNA origami, Nano Lett. **10**, 4756-4761 (2010).
[96] Dai MJ, Jungmann R, Yin P, Optical imaging of individual biomolecules in densely packed clusters, Nat. Nanotech. **11**, 798-807 (2016).

[97] Izeddin I, El Beheiry M, Andilla J, et al., PSF shaping using adaptive optics for three-dimensional single-molecule super-resolution imaging and tracking, Opt. Express **20**, 4957-4967 (2012).
[98] Burke D, Patton B, Huang F, Bewersdorf J, Booth MJ, Adaptive optics correction of specimen-induced aberrations in single-molecule switching microscopy, Optica **2**, 177-185 (2015).
[99] Tehrani KF, Xu J, Zhang Y, Shen P, Kner P, Adaptive optics stochastic optical reconstruction microscopy (AO-STORM) using a genetic algorithm, Opt. Express **23**, 13677-13692 (2015).
[100] Mlodzianoski MJ, Cheng-Hathaway PJ, Bemiller SM, et al., Active PSF shaping and adaptive optics enable volumetric localization microscopy through brain sections, Nat. Methods **15**, 583-586 (2018).
[101] Huang B, Wang WQ, Bates M, Zhuang XW, Three-dimensional super-resolution imaging by stochastic optical reconstruction microscopy, Science **319**, 810-813 (2008).
[102] Pavani SRP, Thompson MA, Biteen JS, et al., Three-dimensional, single-molecule fluorescence imaging beyond the diffraction limit by using a double-helix point spread function, Proc. Natl. Acad. Sci. U.S.A. **106**, 2995-2999 (2009).
[103] Shechtman Y, Sahl SJ, Backer AS, Moerner WE, Optimal point spread function design for 3D imaging, Phys. Rev. Lett. **113**, 133902 (2014).
[104] Jia S, Vaughan JC, Zhuang X, Isotropic three-dimensional super-resolution imaging with a self-bending point spread function, Nat. Photon. **8**, 302-306 (2014).
[105] von Diezmann A, Shechtman Y, Moerner WE, Three-dimensional localization of single molecules for super resolution imaging and single-particle tracking, Chem. Rev. **117**, 7244-7275 (2017).
[106] Agard DA, Optical sectioning microscopy - cellular architecture in 3 dimensions, Annu. Rev. Biophys. Bioeng. **13**, 191-219 (1984).
[107] Neil MAA, Juskaitis R, Wilson T, Method of obtaining optical sectioning by using structured light in a conventional microscope, Opt. Lett. **22**, 1905-1907 (1997).
[108] Axelrod D, Evanescent excitation and emission in fluorescence microscopy, Biophys. J. **104**, 1401-1409 (2013).
[109] Axelrod D, Total internal reflection fluorescence microscopy in cell biology, Traffic **2**, 764-774 (2001).
[110] Roy R, Hohng S, Ha T, A practical guide to single-molecule FRET, Nat. Methods **5**, 507-516 (2008).
[111] Axelrod D, Cell-substrate contacts illuminated by total internal-reflection fluorescence, J. Cell Biol. **89**, 141-145 (1981).
[112] Grandin HM, Stadler B, Textor M, Voros J, Waveguide excitation fluorescence microscopy: A new tool for sensing and imaging the biointerface, Biosens. Bioelectron. **21**, 1476-1482 (2006).
[113] Diekmann R, Helle OI, Oie CI, et al., Chip-based wide field-of-view nanoscopy, Nat. Photon. **11**, 322–328 (2017).
[114] Mattheyses AL, Shaw K, Axelrod D, Effective elimination of laser interference fringing in fluorescence microscopy by spinning azimuthal incidence angle, Micr. Res. Tech. **69**, 642-647 (2006).
[115] Fiolka R, Belyaev Y, Ewers H, Stemmer A, Even illumination in total internal reflection fluorescence microscopy using laser light, Micr. Res. Tech. **71**, 45-50 (2008).
[116] Zong WJ, Huang XS, Zhang C, et al., Shadowless-illuminated variable-angle TIRF (siva-TIRF) microscopy for the observation of spatial-temporal dynamics in live cells, Biomed. Opt. Express **5**, 1530-1540 (2014).
[117] Scholtens TM, Schreuder F, Ligthart ST, et al., CellTracks TDI: An image cytometer for cell characterization, Cytometry Part A **79A**, 203-213 (2011).
[118] Deschamps J, Rowald A, Ries J, Efficient homogeneous illumination and optical sectioning for quantitative single-molecule localization microscopy, Opt. Express **24**, 28080-28090 (2016).
[119] Khaw I, Croop B, Tang J, et al., Flat-field illumination for quantitative fluorescence imaging, Opt. Express **26**, 15276-15288 (2018).
[120] Rowlands CJ, Strohl F, Ramirez PPV, Scherer KM, Kaminski CF, Flat-field super-resolution localization microscopy with a low-cost refractive beam-shaping element, Sci. Rep. **8**, 5630 (2018).
[121] Stehr F, Stein J, Schueder F, Schwille P, Jungmann R, Flat-top TIRF illumination boosts DNA-PAINT imaging and quantification, Nat. Comm. **10**, 1268 (2019).
[122] Brunstein M, Teremetz M, Herault K, Tourain C, Oheim M, Eliminating Unwanted Far-Field Excitation in Objective-Type TIRF. Part I. Identifying Sources of Nonevanescent Excitation Light, Biophys. J. **106**, 1020-1032 (2014).
[123] Brunstein M, Herault K, Oheim M, Eliminating Unwanted Far-Field Excitation in Objective-Type TIRE Part II. Combined Evanescent-Wave Excitation and Supercritical-Angle Fluorescence Detection Improves Optical Sectioning, Biophys. J. **106**, 1044-1056 (2014).
[124] Ruckstuhl T, Verdes D, Supercritical angle fluorescence (SAF) microscopy, Opt. Express **12**, 4246-4254 (2004).
[125] Barroca T, Balaa K, Leveque-Fort S, Fort E, Full-field near-field optical microscope for cell imaging, Phys. Rev. Lett. **108**, 218101 (2012).
[126] Fiolka R, Clearer view for TIRF and oblique illumination microscopy, Opt. Express **24**, 29556-29567 (2016).
[127] Cui BX, Wu CB, Chen L, et al., One at a time, live tracking of NGF axonal transport using quantum dots, Proc. Natl. Acad. Sci. U.S.A. **104**, 13666-13671 (2007).
[128] Guo YT, Li D, Zhang SW, et al., Visualizing Intracellular Organelle and Cytoskeletal Interactions at Nanoscale Resolution on Millisecond Timescales, Cell **175**, 1430-1442 (2018).
[129] Tokunaga M, Imamoto N, Sakata-Sogawa K, Highly inclined thin illumination enables clear single-molecule imaging in cells, Nat. Methods **5**, 159-161 (2008).

[130] Konopka CA, Bednarek SY, Variable-angle epifluorescence microscopy: a new way to look at protein dynamics in the plant cell cortex, Plant J. **53**, 186-196 (2008).
[131] Jungmann R, Avendano MS, Woehrstein JB, et al., Multiplexed 3D cellular super-resolution imaging with DNA-PAINT and Exchange-PAINT, Nat. Methods **11**, 313-318 (2014).
[132] Izeddin I, Recamier V, Bosanac L, et al., Single-molecule tracking in live cells reveals distinct target-search strategies of transcription factors in the nucleus, eLife **3**, e02230 (2014).
[133] van't Hoff M, de Sars V, Oheim M, A programmable light engine for quantitative single molecule TIRF and HILO imaging, Opt. Express **16**, 18495-18504 (2008).
[134] Tang J, Han KY, Extended field-of-view single-molecule imaging by highly inclined swept illumination, Optica **5**, 1063-1069 (2018).
[135] Wilson T, Resolution and optical sectioning in the confocal microscope, J. Microsc. **244**, 113-121 (2011).
[136] Mubaid F, Brown CM, Less is more: Longer exposure times with low light intensity is less photo-toxic, Micros. Today **25**, 26-35 (2017).
[137] Petráň M, Hadravský M, Egger MD, Galambos R, Tandem-scanning reflected-light microscope, J. Opt. Soc. Am. **58**, 661-664 (1968).
[138] McCabe EM, Fewer DT, Ottewill AC, Hewlett SJ, Hegarty J, Direct-view microscopy: Optical sectioning strength for finite-sized, multiple-pinhole arrays, J. Microscopy **184**, 95-105 (1996).
[139] Tanaami T, Otsuki S, Tomosada N, et al., High-speed 1-frame/ms scanning confocal microscope with a microlens and Nipkow disks, Appl. Opt. **41**, 4704-4708 (2002).
[140] Graf R, Rietdorf J, Zimmermann T, "Live cell spinning disk microscopy," in *Microscopy Techniques* (Springer, Berlin, 2005), pp. 57-75.
[141] Egner A, Andresen V, Hell SW, Comparison of the axial resolution of practical Nipkow-disk confocal fluorescence microscopy with that of multifocal multiphoton microscopy: theory and experiment, J. Microsc. **206**, 24-32 (2002).
[142] Egner A, Hell SW, Time multiplexing and parallelization in multifocal multiphoton microscopy, J. Opt. Soc. Am. A **17**, 1192-1201 (2000).
[143] Shimozawa T, Yamagata K, Kondo T, et al., Improving spinning disk confocal microscopy by preventing pinhole cross-talk for intravital imaging, Proc. Natl. Acad. Sci. U.S.A. **110**, 3399-3404 (2013).
[144] Sheppard CJR, Mao XQ, Confocal microscopes with slit apertures, J. Mod. Opt. **35**, 1169-1185 (1988).
[145] Brakenhoff GJ, Visscher K, Confocal imaging with bilateral scanning and array detectors, J. Microsc. **165**, 139-146 (1992).
[146] Wolleschensky R, Zimmermann B, Kempe M, High-speed confocal fluorescence imaging with a novel line scanning microscope, J. Biomed. Opt. **11**, 064011 (2006).
[147] Fiolka R, Stemmer A, Belyaev Y, Virtual slit scanning microscopy, Histochem Cell Biol **128**, 499-505 (2007).
[148] Lee J, Miyanaga Y, Ueda M, Hohng S, Video-rate confocal microscopy for single-molecule imaging in live cells and superresolution fluorescence imaging, Biophys. J. **103**, 1691-1697 (2012).
[149] Park S, Kang W, Kwon YD, et al., Superresolution fluorescence microscopy for 3D reconstruction of thick samples, Mol. Brain **11**, 17 (2018).
[150] Yang T, Zheng T, Shang ZH, et al., Rapid imaging of large tissues using high-resolution stage-scanning microscopy, Biomed. Opt. Express **6**, 1867-1875 (2015).
[151] Gareau DS, Krueger JG, Hawkes JE, et al., Line scanning, stage scanning confocal microscope (LSSSCM), Biomed. Opt. Express **8**, 3807-3815 (2017).
[152] Mei E, Fomitchov PA, Graves R, Campion M, A line scanning confocal fluorescent microscope using a CMOS rolling shutter as an adjustable aperture, J. Microsc. **247**, 269-276 (2012).
[153] Brakenhoff GJ, Squier J, Norris T, et al., Real-time two-photon confocal microscopy using a femtosecond, amplified Ti:sapphire system, J. Microsc. **181**, 253-259 (1996).
[154] Tang J, Han KY, Low-photobleaching line-scanning confocal microscopy using dual inclined beams, J. Biophotonics, e201900075 (2019).
[155] Voie AH, Burns DH, Spelman FA, Orthogonal-plane fluorescence optical sectioning - 3-dimensional imaging of macroscopic biological specimens, J. Microsc. **170**, 229-236 (1993).
[156] Fuchs E, Jaffe JS, Long RA, Azam F, Thin laser light sheet microscope for microbial oceanography, Opt. Express **10**, 145-154 (2002).
[157] Huisken J, Swoger J, Del Bene F, Wittbrodt J, Stelzer EHK, Optical sectioning deep inside live embryos by selective plane illumination microscopy, Science **305**, 1007-1009 (2004).
[158] Power RM, Huisken J, A guide to light-sheet fluorescence microscopy for multiscale imaging, Nat. Methods **14**, 360-373 (2017).
[159] Keller PJ, Schmidt AD, Wittbrodt J, Stelzer EHK, Reconstruction of zebrafish early embryonic development by scanned light sheet microscopy, Science **322**, 1065-1069 (2008).
[160] Huisken J, Stainier DYR, Even fluorescence excitation by multidirectional selective plane illumination microscopy (mSPIM), Opt. Lett. **32**, 2608-2610 (2007).
[161] Krzic U, Gunther S, Saunders TE, Streichan SJ, Hufnagel L, Multiview light-sheet microscope for rapid *in toto* imaging, Nat. Methods **9**, 730-733 (2012).
[162] Durnin J, Miceli JJ, Eberly JH, Diffraction-free beams, Phys. Rev. Lett. **58**, 1499-1501 (1987).

[163] Fahrbach FO, Simon P, Rohrbach A, Microscopy with self-reconstructing beams, Nat. Photon. **4**, 780-785 (2010).
[164] Planchon TA, Gao L, Milkie DE, et al., Rapid three-dimensional isotropic imaging of living cells using Bessel beam plane illumination, Nat. Methods **8**, 417-423 (2011).
[165] Fahrbach FO, Rohrbach A, A line scanned light-sheet microscope with phase shaped self-reconstructing beams, Opt. Express **18**, 24229-24244 (2010).
[166] Belanger PA, Rioux M, Ring pattern of a lens-axicon doublet illuminated by a Gaussian-beam, Appl. Opt. **17**, 1080-1086 (1978).
[167] Fahrbach FO, Rohrbach A, Propagation stability of self-reconstructing Bessel beams enables contrast-enhanced imaging in thick media, Nat. Comm. **3**, 632 (2012).
[168] Zhang P, Phipps ME, Goodwin PM, Werner JH, Confocal line scanning of a Bessel beam for fast 3D Imaging, Opt. Lett. **39**, 3682-3685 (2014).
[169] Betzig E, Sparse and composite coherent lattices, Phys. Rev. A **71**, 063406 (2005).
[170] Chen B-C, Legant WR, Wang K, et al., Lattice light-sheet microscopy: Imaging molecules to embryos at high spatiotemporal resolution, Science **346**, 439 (2014).
[171] Mori S, Side lobe suppression of a Bessel beam for high aspect ratio laser processing, Precis. Eng. **39**, 79-85 (2015).
[172] Di Domenico G, Ruocco G, Colosi C, Delre E, Antonacci G, Cancellation of Bessel beam side lobes for high-contrast light sheet microscopy, Sci. Rep. **8**, 17178 (2018).
[173] Golub I, Chebbi B, Golub J, Toward the optical "magic carpet": reducing the divergence of a light sheet below the diffraction limit, Opt. Lett. **40**, 5121-5124 (2015).
[174] Fadero TC, Gerbich TM, Rana K, et al., LITE microscopy: Tilted light-sheet excitation of model organisms offers high resolution and low photobleaching, J. Cell. Biol. **217**, 1869-1882 (2018).
[175] Siviloglou GA, Broky J, Dogariu A, Christodoulides DN, Observation of accelerating airy beams, Phys. Rev. Lett. **99**, 213901 (2007).
[176] Vettenburg T, Dalgarno HIC, Nylk J, et al., Light-sheet microscopy using an Airy beam, Nat. Methods **11**, 541-544 (2014).
[177] Dean KM, Roudot P, Welf ES, Danuser G, Fiolka R, Deconvolution-free subcellular imaging with axially swept light sheet microscopy, Biophys. J. **108**, 2807-2815 (2015).
[178] Gao L, Extend the field of view of selective plan illumination microscopy by tiling the excitation light sheet, Opt. Express **23**, 6102-6111 (2015).
[179] Yang Z, Mei L, Xia F, et al., Dual-slit confocal light sheet microscopy for in vivo whole-brain imaging of zebrafish, Biomed. Opt. Express **6**, 1797-1811 (2015).
[180] Chang B-J, Kittisopikul M, Dean KM, et al., Universal light-sheet generation with field synthesis, Nat. Methods **16**, 235-238 (2019).
[181] Zhao T, Lau SC, Wang Y, et al., Multicolor 4D fluorescence microscopy using ultrathin bessel light sheets, Sci. Rep. **6**, 26159 (2016).
[182] Gao L, Shao L, Higgins CD, et al., Noninvasive imaging beyond the diffraction limit of 3D dynamics in thickly fluorescent specimens, Cell **151**, 1370-1385 (2012).
[183] Friedrich M, Gan Q, Ermolayev V, Harms GS, STED-SPIM: Stimulated emission depletion improves sheet illumination microscopy resolution, Biophys. J. **100**, L43-L45 (2011).
[184] Hoyer P, de Medeiros G, Balazs B, et al., Breaking the diffraction limit of light-sheet fluorescence microscopy by RESOLFT, Proc. Natl. Acad. Sci. U.S.A. **113**, 3442-3446 (2016).
[185] Wilding D, Pozzi P, Soloviev O, Vdovin G, Verhaegen M, Adaptive illumination based on direct wavefront sensing in a light-sheet fluorescence microscope, Opt. Express **24**, 24896-24906 (2016).
[186] Bourgenot C, Saunter CD, Taylor JM, Girkin JM, Love GD, 3D adaptive optics in a light sheet microscope, Opt. Express **20**, 13252-13261 (2012).
[187] Royer LA, Lemon WC, Chhetri RK, et al., Adaptive light-sheet microscopy for long-term, high-resolution imaging in living organisms, Nat. Biotechnol. **34**, 1267-1278 (2016).
[188] Ritter JG, Veith R, Veenendaal A, Siebrasse JP, Kubitscheck U, Light sheet microscopy for single molecule tracking in living tissue, PLoS One **5**, e11639 (2010).
[189] Zanacchi FC, Lavagnino Z, Donnorso MP, et al., Live-cell 3D super-resolution imaging in thick biological samples, Nat. Methods **8**, 1047-1049 (2011).
[190] Gustavsson AK, Petrov PN, Moerner WE, Light sheet approaches for improved precision in 3D localization-based super-resolution imaging in mammalian cells [Invited], Opt. Express **26**, 13122-13147 (2018).
[191] Gebhardt JCM, Suter DM, Roy R, et al., Single-molecule imaging of transcription factor binding to DNA in live mammalian cells, Nat. Methods **10**, 421-426 (2013).
[192] Galland R, Grenci G, Aravind A, et al., 3D high- and super-resolution imaging using single-objective SPIM, Nat. Methods **12**, 641-644 (2015).
[193] Meddens MBM, Liu S, Finnegan PS, et al., Single objective light-sheet microscopy for high-speed whole-cell 3D super-resolution, Biomed. Opt. Express **7**, 2219-2236 (2016).
[194] Hu YS, Zhu Q, Elkins K, et al., Light-sheet Bayesian microscopy enables deep-cell super-resolution imaging of heterochromatin in live human embryonic stem cells, Optical Nanoscopy **2**, 7 (2013).

[195] Strnad P, Gunther S, Reichmann J, et al., Inverted light-sheet microscope for imaging mouse pre-implantation development, Nat. Methods **13**, 139-142 (2016).
[196] Gustavsson AK, Petrov PN, Lee MY, Shechtman Y, Moerner WE, 3D single-molecule super-resolution microscopy with a tilted light sheet, Nat. Comm. **9**, 123 (2018).
[197] Dunsby C, Optically sectioned imaging by oblique plane microscopy, Opt. Express **16**, 20306-20316 (2008).
[198] Bouchard MB, Voleti V, Mendes CS, et al., Swept confocally-aligned planar excitation (SCAPE) microscopy for high-speed volumetric imaging of behaving organisms, Nat. Photon. **9**, 113-119 (2015).
[199] Yang B, Chen XY, Wang YN, et al., Epi-illumination SPIM for volumetric imaging with high spatial-temporal resolution, Nat. Methods **16**, 501-504 (2019).
[200] Kim J, Wojcik M, Wang Y, et al., Oblique-plane single-molecule localization microscopy for tissues and small intact animals, Nat. Methods **16**, 853-857 (2019).
[201] Weisenburger S, Vaziri A, A Guide to Emerging Technologies for Large-Scale and Whole-Brain Optical Imaging of Neuronal Activity, Annu. Rev. Neurosci. **41**, 431-452 (2018).
[202] Denk W, Strickler JH, Webb WW, Two-photon laser scanning fluorescence microscopy, Science **248**, 73-76 (1990).
[203] Zong WJ, Wu RL, Li ML, et al., Fast high-resolution miniature two-photon microscopy for brain imaging in freely behaving mice, Nat. Methods **14**, 713-719 (2017).
[204] Theriault G, Cottet M, Castonguay A, McCarthy N, De Koninck Y, Extended two-photon microscopy in live samples with Bessel beams: steadier focus, faster volume scans, and simpler stereoscopic imaging, Front. Cell. Neurosci. **8**, 139 (2014).
[205] Lu RW, Sun WZ, Liang YJ, et al., Video-rate volumetric functional imaging of the brain at synaptic resolution, Nat. Neurosci. **20**, 620-628 (2017).
[206] Cheng A, Gonçalves JT, Golshani P, Arisaka K, Portera-Cailliau C, Simultaneous two-photon calcium imaging at different depths with spatiotemporal multiplexing, Nat. Methods **8**, 139-142 (2011).
[207] Oron D, Tal E, Silberberg Y, Scanningless depth-resolved microscopy, Opt. Express **13**, 1468-1476 (2005).
[208] Zhu GH, van Howe J, Durst M, Zipfel W, Xu C, Simultaneous spatial and temporal focusing of femtosecond pulses, Opt. Express **13**, 2153-2159 (2005).
[209] Dana H, Shoham S, Numerical evaluation of temporal focusing characteristics in transparent and scattering media, Opt. Express **19**, 4937-4948 (2011).
[210] McCabe DJ, Tajalli A, Austin DR, et al., Spatio-temporal focusing of an ultrafast pulse through a multiply scattering medium, Nat. Comm. **2**, 447 (2011).
[211] Tal E, Oron D, Silberberg Y, Improved depth resolution in video-rate line-scanning multiphoton microscopy using temporal focusing, Opt. Lett. **30**, 1686-1688 (2005).
[212] Dana H, Kruger N, Ellman A, Shoham S, Line temporal focusing characteristics in transparent and scattering media, Opt. Express **21**, 5677-5687 (2013).
[213] Rupprecht P, Prevedel R, Groessl F, Haubensak WE, Vaziri A, Optimizing and extending light-sculpting microscopy for fast functional imaging in neuroscience, Biomed. Opt. Express **6**, 353-368 (2015).
[214] Schrodel T, Prevedel R, Aumayr K, Zimmer M, Vaziri A, Brain-wide 3D imaging of neuronal activity in Caenorhabditis elegans with sculpted light, Nat. Methods **10**, 1013-1020 (2013).
[215] Prevedel R, Verhoef AJ, Pernia-Andrade AJ, et al., Fast volumetric calcium imaging across multiple cortical layers using sculpted light, Nat. Methods **13**, 1021-1028 (2016).
[216] Dowski ER, Cathey WT, Extended depth of field through wave-front coding, Appl. Opt. **34**, 1859-1866 (1995).
[217] Quirin S, Peterka DS, Yuste R, Instantaneous three-dimensional sensing using spatial light modulator illumination with extended depth of field imaging, Opt. Express **21**, 16007-16021 (2013).
[218] Quirin S, Vladimirov N, Yang C-T, et al., Calcium imaging of neural circuits with extended depth-of-field light-sheet microscopy, Opt. Lett. **41**, 855-858 (2016).
[219] Abrahamsson S, Chen JJ, Hajj B, et al., Fast multicolor 3D imaging using aberration-corrected multifocus microscopy, Nat. Methods **10**, 60-63 (2013).
[220] Blanchard PM, Greenaway AH, Simultaneous multiplane imaging with a distorted diffraction grating, Appl. Opt. **38**, 6692-6699 (1999).
[221] Hajj B, Wisniewski J, El Beheiry M, et al., Whole-cell, multicolor superresolution imaging using volumetric multifocus microscopy, Proc. Natl. Acad. Sci. U.S.A. **111**, 17480-17485 (2014).
[222] Rubinsztein-Dunlop H, Forbes A, Berry MV, et al., Roadmap on structured light, J. Opt. **19**, 013001 (2017).
[223] Duocastella M, Arnold CB, Bessel and annular beams for materials processing, Laser Photonics Rev. **6**, 607-621 (2012).
[224] Fischer J, Wegener M, Three-dimensional optical laser lithography beyond the diffraction limit, Laser Photonics Rev. **7**, 22-44 (2013).
[225] Grier DG, A revolution in optical manipulation, Nature **424**, 810-816 (2003).
[226] MacDonald MP, Spalding GC, Dholakia K, Microfluidic sorting in an optical lattice, Nature **426**, 421-424 (2003).
[227] Vaziri A, Emiliani V, Reshaping the optical dimension in optogenetics, Curr. Opin. Neurobiol. **22**, 128-137 (2012).

Figures

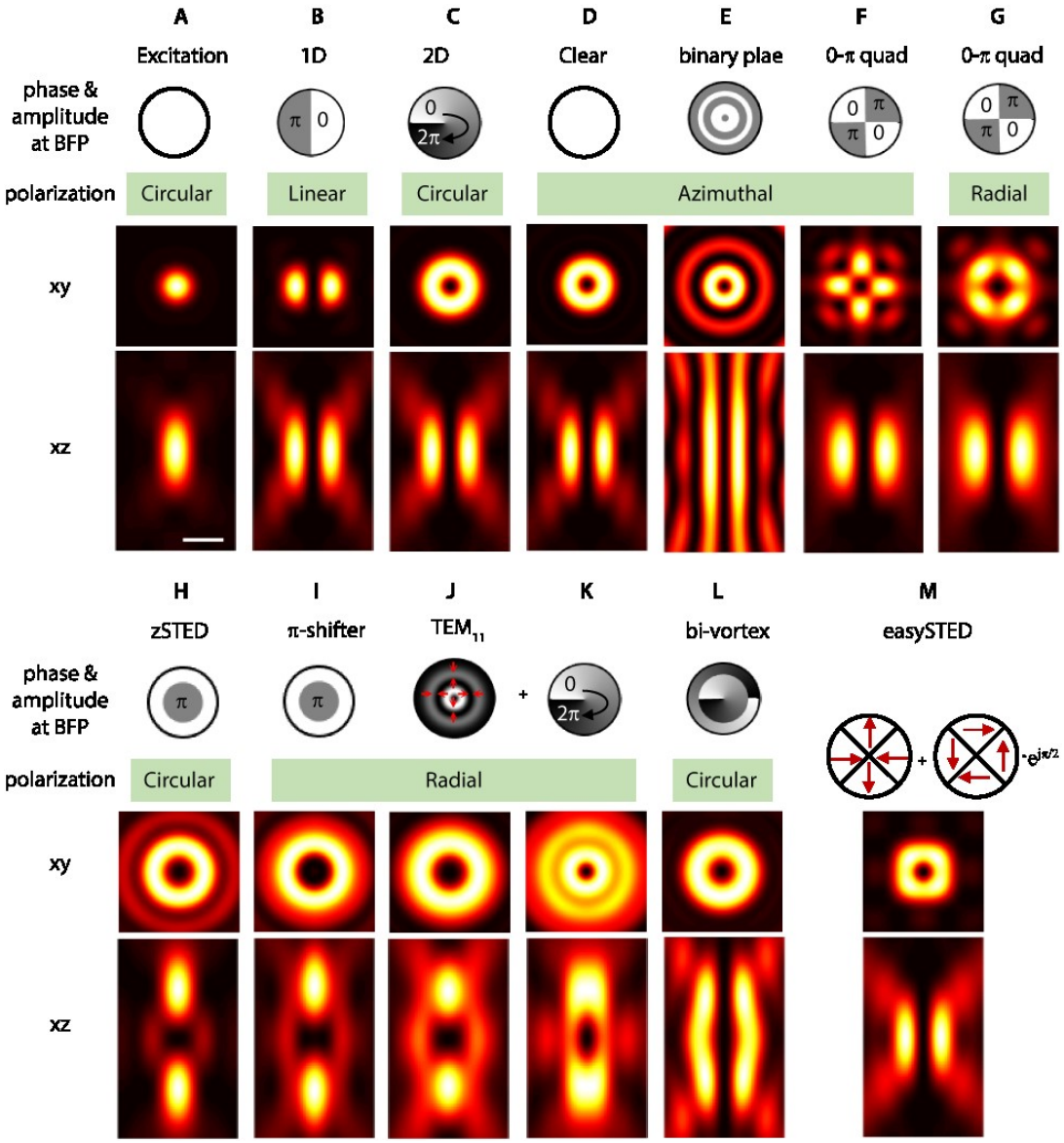

Figure 1: PSF engineering of tightly focused STED beams.
Beam intensity distributions in the *xy* and *xz* planes with various phases and polarization states at a pupil plane of objective. (A) Gaussian beam with circular polarization. (B) Linearly polarized 1D-STED pattern generated by a semi-circular π-shifting phase plate, where the linear polarization is parallel to the dividing line of the phase plate. (C) A doughnut pattern (2D-STED) through a phase vortex using a circularly polarized beam. (D-G) Depletion patterns using cylindrical vector beams. Azimuthally polarized beams through a clear aperture (D), binary phase plate (E) or quadrant $0/\pi$ phase plate (F). A radially polarized beam through a quadrant $0/\pi$ phase plate (G). (H,I) Axially confined patterns through a π-shifter with a circularly (H) or radially (I) polarized beam. 3D de-excitation patterns can be generated by incoherently superposing C and H as well as G and I. (J,K) Optical cage patterns for isotropic 3D-STED using a higher-order radially polarized transverse electromagnetic mode (TEM_{11}) in (J) combined with a vortex phase plate (K). (L) Coherent hybrid depletion pattern generated by two out-of-phase vortices. (M) Alignment-free easySTED using an achromatic quarter waveplate and a chromatic segmented half waveplate. Polarization states are displayed at two different wave cycles. A wavelength of STED beam = 775 nm, objective NA = 1.4, refractive index (*n*) of medium = 1.518. Scale bar, 500 nm.

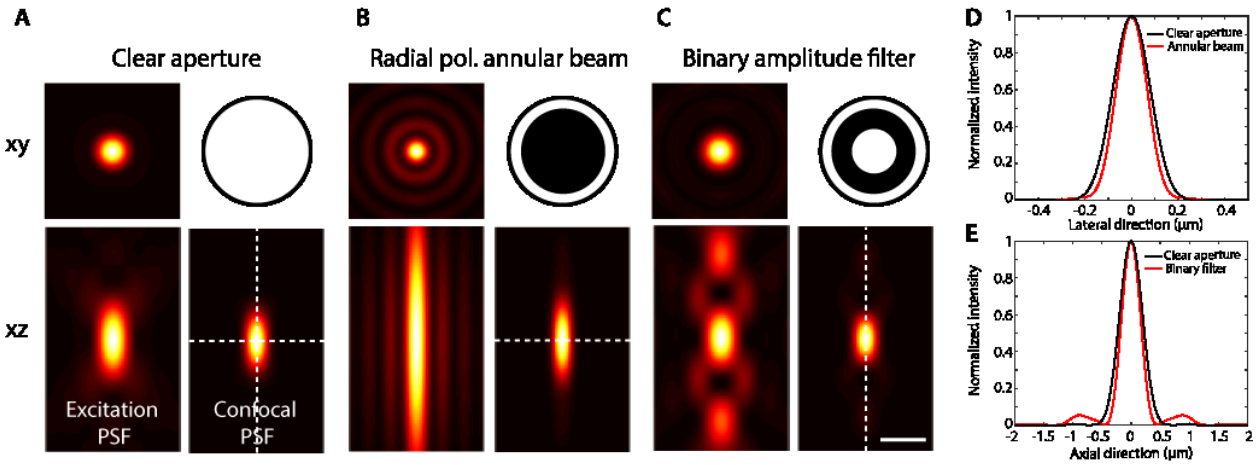

Figure 2: Sharper excitation beams for STED microscopy.
Excitation and confocal point spread functions (PSF) of a circularly polarized beam through a clear aperture (A), a radially polarized annular beam for lateral resolution enhancement (B), and a circularly polarized beam through a binary amplitude filter for axial resolution enhancement (C). (D) Lateral profiles of confocal PSF with the clear aperture (black) and radially polarized annular beam (red). (E) Axial profiles of confocal PSF with the clear aperture (black) and binary amplitude filter (red). 1 Airy unit is used as a confocal pinhole size. Scale bar, 500 nm.

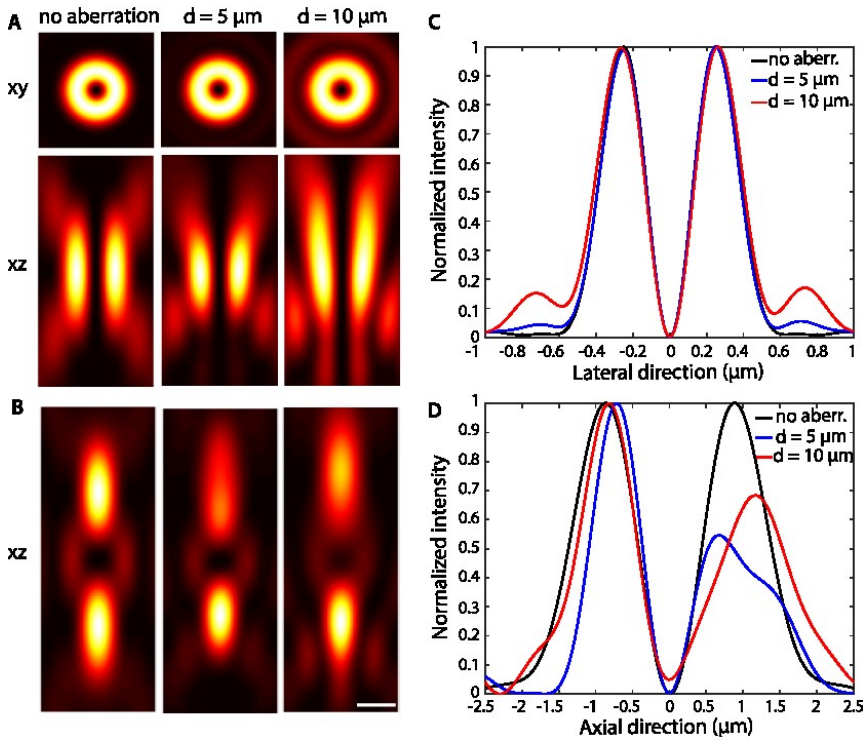

Figure 3: Aberration in STED beams.
Influence of the aberration induced by refractive index mismatch in the sample for 2D-STED and z-STED. Intensity distributions in the xz plane and line profiles for an aberration-free case and different imaging depths indicated by *d*. Clearly, compared to 2D-STED, z-STED is more susceptible to aberrations, including the degradation of the symmetricity of PSF shape and considerable amount of the residual intensity at the center as the increasing imaging depths. Since the index mismatch causes the focus shift, for better comparison, all profiles are shifted accordingly to keep the minimal intensity at the origin. Scale bar, 500 nm.

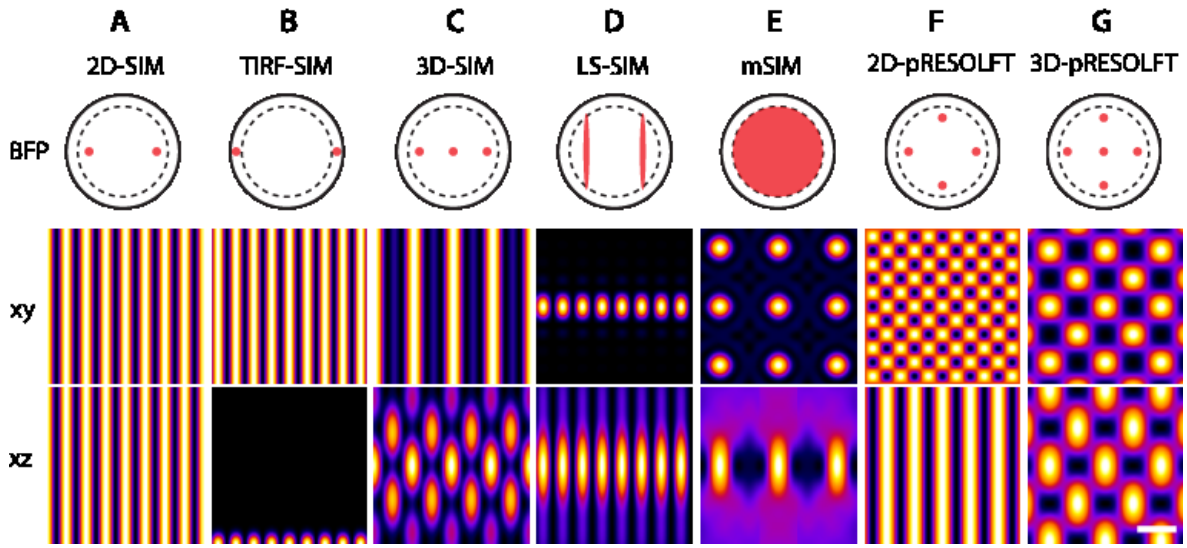

Figure 4: Beam shaping for SIM and parallelized RESOLFT.
Comparison of beam positions at the back focal plane (BFP) and intensity distributions on the xy and xz planes for each method. At the BFP, the dashed circle denotes the critical angle position assuming a glass/water interface. The red dots indicate focused beams at BFP. (A) 2D-SIM, two-dimensional structured illumination microscopy with a sinusoidal illumination pattern on the xy plane. (B) TIRF-SIM, SIM with total internal reflection fluorescence illumination. (C) 3D-SIM, 3D illumination pattern generated by interference of three beams. (D) LS-SIM, SIM with a line-scan pattern generated by interference of two lines. (E) mSIM, multifocal SIM with multiple focused spots. (F) 2D-pRESOLFT, two-dimensional parallelized reversible saturable optical fluorescence transitions microscopy. Two orthogonally structured illumination patterns are incoherently superimposed on the sample plane. (G) 3D-pRESOLFT, three dimensional parallelized RESOLFT generated by interference of five coherent beams. All the beams are *s*-polarized except E and G, which are circularly polarized. Scale bar, 500 nm.

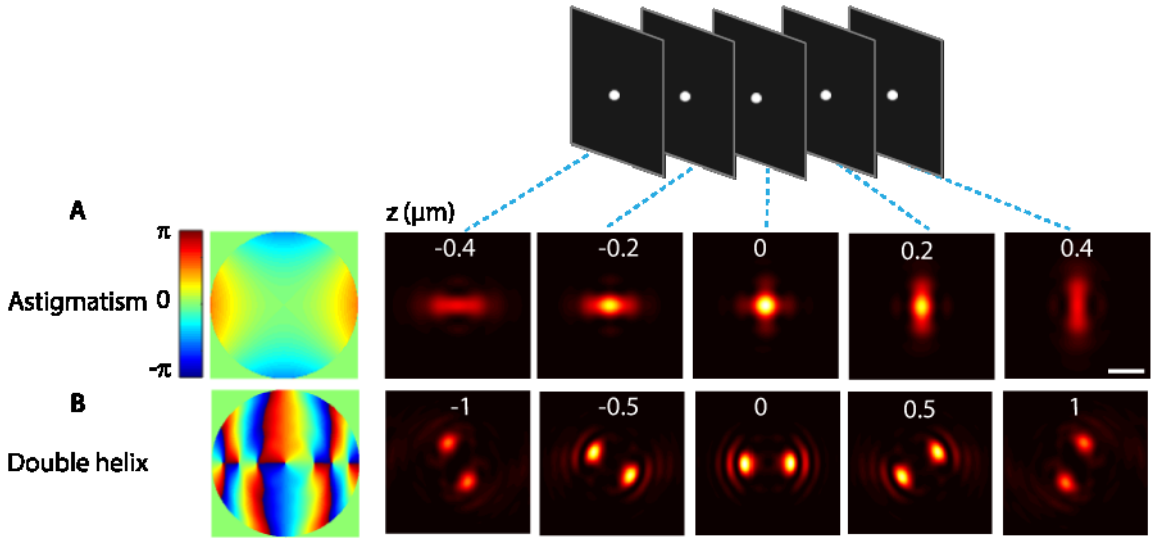

Figure 5: PSF engineering for encoding the fluorescent emitter's depth information.
(A) Astigmatic phase mask on the back focal plane and PSF intensity distribution at the different imaging depths, where the PSF widths along x and y axes vary as a function of defocusing depth. (B) Double-helix phase mask and PSF intensity distribution, where the angle of two main PSF lobes is characterized as a distinguishable parameter for encoded imaging depths. Scale bar, 1 μm.

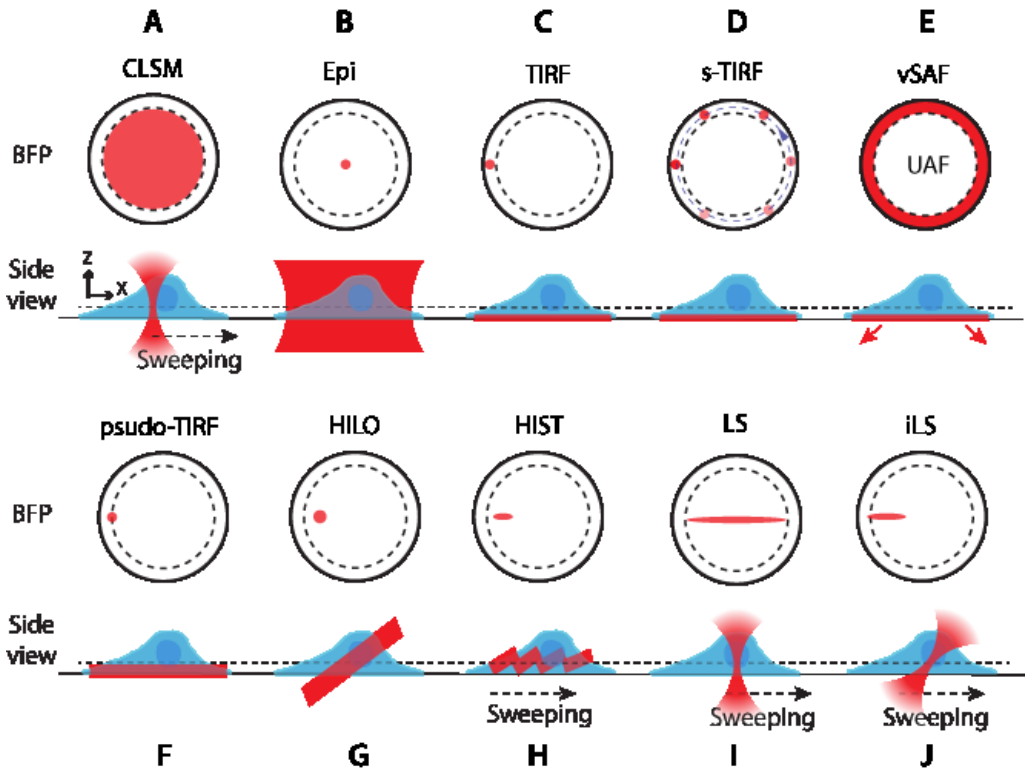

Figure 6: Background suppression schemes for different imaging systems.
(A) CLSM, confocal laser scanning microscopy. (B) Epi, epi-illumination widefield microscopy. A beam focused at the center of BFP excites an entire imaging volume. (C) TIRF, total internal reflection fluorescence microscopy. A beam is focused to the edge of BFP. (D) s-TIRF, spinning TIRF generates uniform illumination by rotating the focused spot. (E) vSAF, virtual supercritical angle fluorescence. TIRF-like imaging is achieved by the subtraction of undercritical angle fluorescence (UAF) from all emission components. (F) psudo-TIRF with a deeper penetration depth of ~ 1 μm. (G) HILO, highly inclined and laminated optical sheet. Inclined illumination with a small FOV is typically used for minimizing out-of-focus background. (H) HIST, highly inclined swept tile microscopy. Inclined tile beam ensures a thinner illumination and larger FOV than HILO. Full FOV imaging is achieved by sweeping the tile together with a confocal slit detection. (I) LS, line-scanning confocal microscopy. Out-of-focus background fluorescence is rejected by a slit. (J) iLS, inclined line-scanning confocal microscopy. Inclined focused line is used for sample illumination with much lower illumination intensity than LS.

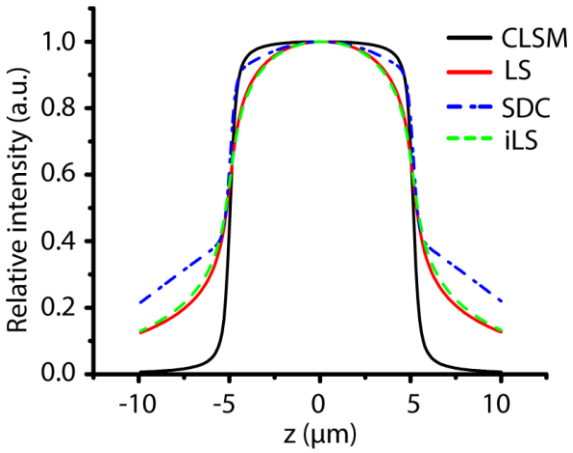

Figure 7: Optical sectioning of confocal microscopy and its variants.
z-responses of a fluorescent sample with 10 µm thickness for point-scanning (CLSM, solid black), line-scanning (LS, solid red), spinning disk (SDC, dashed blue) and inclined line-scanning (iLS, dashed green) confocal microscopy. SDC shows the highest offset background level due to a strong crosstalk between pinholes.

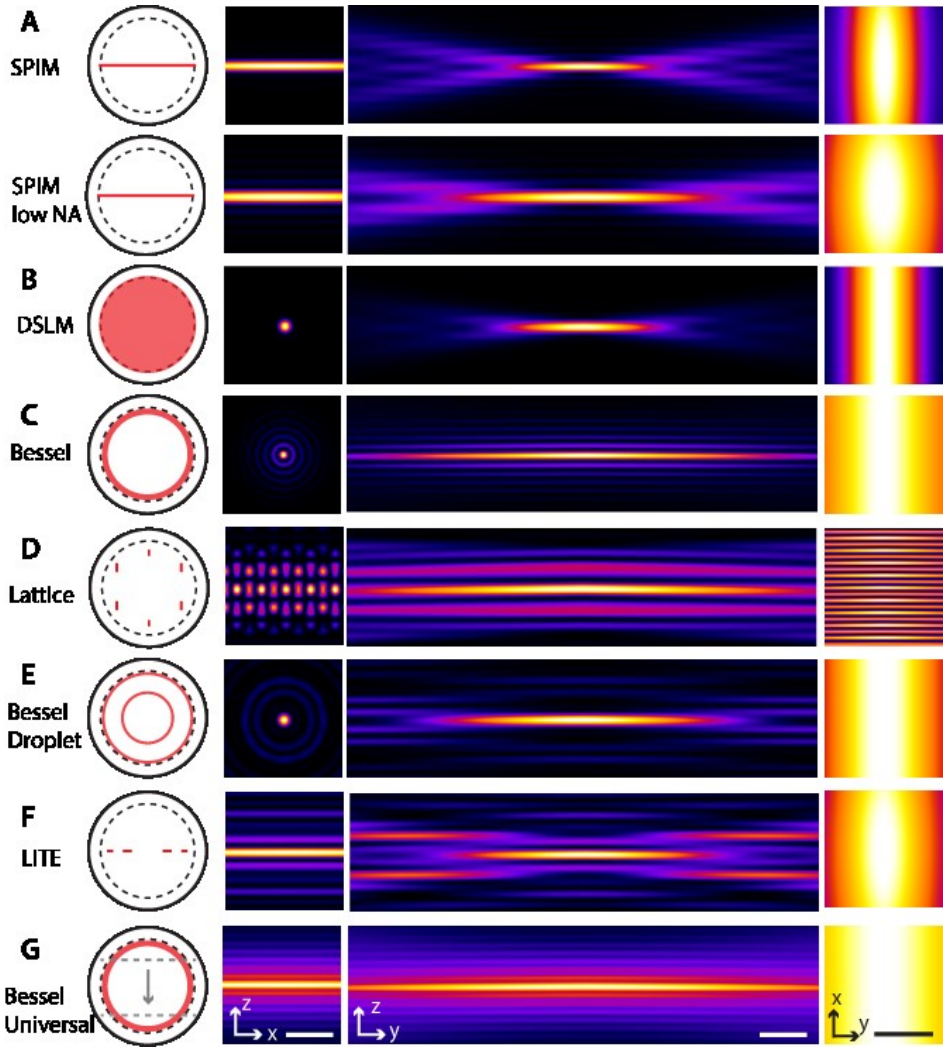

Figure 8: Beam shaping for light-sheet fluorescence microscopy.
(A) SPIM, selective plane illumination microscopy. A thicker beam is required to generate a larger FOV light-sheet with a low NA objective. (B) DSLM, digital scanned laser light-sheet fluorescence microscopy. A pencil-like excitation beam is scanned across FOV. (C) Bessel, Bessel beam light-sheet microcopy for generating thin illumination and large FOV. (D) Lattice, lattice light-sheet microscopy. (E) Bessel droplet, Side lobes of the Bessel beam are minimized by the interference of two beams. (F) LITE, lateral interference tilted excitation. (G) Universal light-sheet generation. Any scanned or dithered light-sheet illumination can be synthesized by scanning the aperture of BFP with a focused line. An example here is a synthesized Bessel beam. Scale bars, 2 μm (xz and yz planes), 5 μm (xy plane).